ADVANCED FUNCTIONAL MATERIALS
www.afm-journal.de

Multicolored Nanocolloidal Hydrogel Inks

*Sofia M. Morozova, Tatiana G. Statsenko, Egor O. Ryabchenko, Albert Gevorkian, Vahid Adibnia, Maksim S. Lozhkin, Alexey V. Kireynov, and Eugenia Kumacheva**

Nanocolloidal gels are emerging as a promising class of materials with applications as inks in 2D and 3D printing. Polymer nanoparticles (NPs) offer many advantages as potential building blocks of nanocolloidal gels, due to the ability to control NP dimensions, charge, surface chemistry, and functionality; however, their applications as inks in printing are yet to be explored. Here, functional nanocolloidal hydrogels formed by percolating oppositely charged latex NPs with different dimensions and charge densities are reported. The shear-thinning and self-healing properties of the nanocolloidal gels and the mechanical properties of the resulting printed films are examined. NP functionality is achieved by covalently labeling them with different fluorescent dyes that emit at two distinct wavelengths. Using these NPs, a facile route for 3D printing of multicolored fluorescence patterns is shown, with each color being visualized under a specific, well-defined excitation wavelength.

1. Introduction

Nanocolloidal gels are composed of a continuous network containing at least, one nanoparticle (NP) component.[1–10] Owing to a great level of control over their stability, structure, elasticity and rheological properties, as well as NP functionality,[11,12] physically cross-linked nanocolloidal gels have promising applications as "inks" for extrusion-based 3D printing, that is, the fabrication of objects by digitally controlled layer-by-layer deposition of liquid precursors.[13] Patterns printed in functional materials on length scales varying from micrometers to millimeters are utilized in cell culture, tissue engineering, optics, anticounterfeiting technologies, and the generation of quick response codes and barcodes.[14–16] While both inkjet printing and extrusion-based printing are used for large-area patterning and deposition of multicomponent inks,[17] extrusion-based 3D printing enables the fabrication of 3D objects, provides the capability of shear-induced alignment of shape-anisotropic NPs,[18] and is extensively used for bioprinting.

The utilization of nanocolloidal gel inks offers almost unlimited possibilities for the fabrication of organic, inorganic, and hybrid materials with multiscale hierarchical structures and compositions. Transient reversible physical interactions such as hydrogen bonding, electrostatic attraction, or hydrophobic forces between gel components can lead to shear thinning (thixotropy),[1] with viscosity reducing at increasing shear rate.[19] This property allows a gel ink to flow smoothly and continuously under relatively low shear stresses. On the other hand, fast viscosity recovery of the gel after the shear is ceased (that is, the "self-healing" behavior) provides the ability to retain ink shape after the shear is ceased and preserve shear-induced orientation of ink components in the extruded material.[7]

The ability to change independently the dimensions, charge, surface chemistry, and functionality of polymer latex NPs makes them promising building blocks of nanocolloidal gels, as it enables systematic studies of the role of interparticle

S. M. Morozova, T. G. Statsenko, A. V. Kireynov
N. E. Bauman Moscow State Technical University
5/1 2nd Baumanskaya Street, Moscow 105005, Russia
S. M. Morozova, T. G. Statsenko, E. O. Ryabchenko, E. Kumacheva
Biochemistry cluster
International Institute "Solution Chemistry of Advanced Materials and Technologies" (SCAMT) 9
ITMO University
Lomonosova Street, Saint Petersburg 191002, Russia
A. Gevorkian, V. Adibnia, E. Kumacheva
Department of Chemistry
University of Toronto
80 Saint George Street, Toronto, Ontario M5S 3H6, Canada
E-mail: eugenia.kumacheva@utoronto.ca
M. S. Lozhkin
Saint Petersburg State University
1 Ulyanovskaya Street, Saint Petersburg 198504, Russia
E. Kumacheva
Department of Chemical Engineering and Applied Chemistry
University of Toronto
200 College Street, Toronto, Ontario M5S 3E5, Canada
E. Kumacheva
The Institute of Biomaterials and Biomedical Engineering
University of Toronto
4 Taddle Creek Road, Toronto, Ontario M5S 3G9, Canada
The ORCID identification number(s) for the author(s) of this article can be found under https://doi.org/10.1002/adfm.202105470.

DOI: 10.1002/adfm.202105470

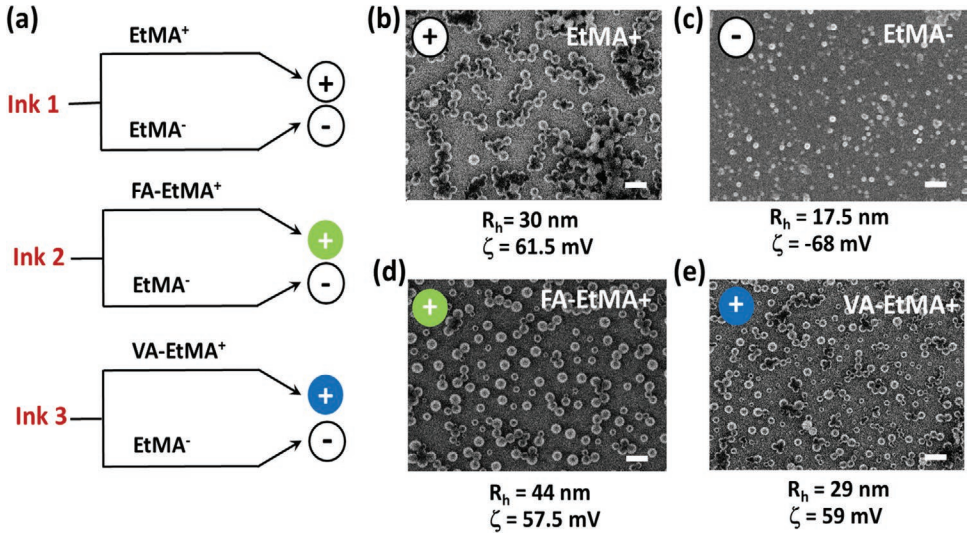

Figure 1. Building blocks of nanocolloidal gels. a) Schematics of the preparation of the gel from oppositely charged latex NPs. b–e) SEM images of optically inactive EtMa+ NPs (b), optically inactive EtMA– NPs (c), optically active FA-EtMa+ NPs (d), and optically active VA-EtMa+ NPs (e). Scale bar is 200 nm.

interactions in percolation transitions. From the practical standpoint, aqueous latex NP dispersions can be used for the preparation of films and coatings from both hydrophilic and hydrophobic polymers,[20–23] with applications as paints,[24] films for biometrics and optical data storage,[25–28] self-healing coatings,[29] and membranes.[30] Importantly, in such systems, high molecular weight polymers can be used without increase in dispersion viscosity.[31] Despite the fact that the thixotropy of latex dispersions has been known for a long time and even used in inkjet printing,[32] nanocolloidal hydrogel inks formed solely from attractive percolating latex NPs have not been reported for 3D printing of functional materials.

In the present work, we report functional nanocolloidal gel inks formed by attractive latex NPs percolating in a particular range of NP number densities, dependent on NP sizes, and charge densities. We show that these gels exhibit shear thinning and self-healing properties and use them as inks for extrusion-based 3D printing of polymer films. Ink functionality was achieved by covalently labeling NPs with different fluorescent dyes, thereby achieving photoluminescence (PL) emission at two distinct wavelengths. Using these NPs, we printed polymer films with multicolored patterns, each being visualized using different distinct, well-defined excitation wavelengths. This work is concluded with a discussion of the criteria for the applications of functional polymer nanocolloidal gels as inks for 3D printing.

2. Results and Discussion

2.1. Building Blocks of Nanocolloidal Gel Inks

We rationalized that oppositely charged latex NPs can form a network and nanocolloidal hydrogel, due to electrostatic attraction between the positively and negatively charged NPs, and that subsequently, this hydrogel can be used as a shear thinning ink for extrusion-based 3D printing. **Figure 1**a illustrates the approach to the preparation of NP-based gel inks, while **Table 1** shows the NP properties.

Inks 1–3 were formed by mixing positively and negatively charged latex NPs, all synthesized by emulsion polymerization of ethyl methacrylate (EtMA).[33] Cetyl trimethylammonium bromide (CTAB) and sodium dodecyl sulfate (SDS) were used as surfactants during NP synthesis, thereby tailoring to the NPs positive and negative charges, respectively. 2-2-azo-bis(2-methylpropionamidine) dihydrochloride (V-50) and potassium persulfate (KPS) were used as the initiators for the synthesis of these NPs, respectively.

Furthermore, two populations of NPs were covalently labeled with fluorescent dyes. Positively charged NPs were synthesized by copolymerizing EtMA with o-fluorescein acrylate (FA), while negatively charged NPs were synthesized by copolymerizing EtMA with 9-vinyl anthracene (VA). Overall, four types of NPs

Table 1. Properties of latex NP-based inks.

Sample	Positively charged NPs				Negatively charged NPs				Dye	$\lambda_{ex}/\lambda_{em}$ [nm][d]
	NP type	R_h [nm][a]	ζ [mV][b]	σ [mC m^{-2}][c]	NP type	R_h [nm]	ζ [mV]	σ [mC m^{-2}]		
Ink 1	EtMA+	30	62	2.2	EtMA–	17.5	–68	–4.2	no	no
Ink 2	FA-EtMA+	44	57.5	1.6	EtMA–	17.5	–68	–4.2	o-fluorescein acrylate (FA)	450/526
Ink 3	VA-EtMA+	29	59	2.7	EtMA–	17.5	–68	–4.2	9-vinyl anthracene (VA)	257/428

[a] R_h = hydrodynamic radius; [b] ζ = zeta-potential; [c] σ = charge density; [d] λ_{ex} and λ_{em} wavelength of excitation and emission of the respective dye.

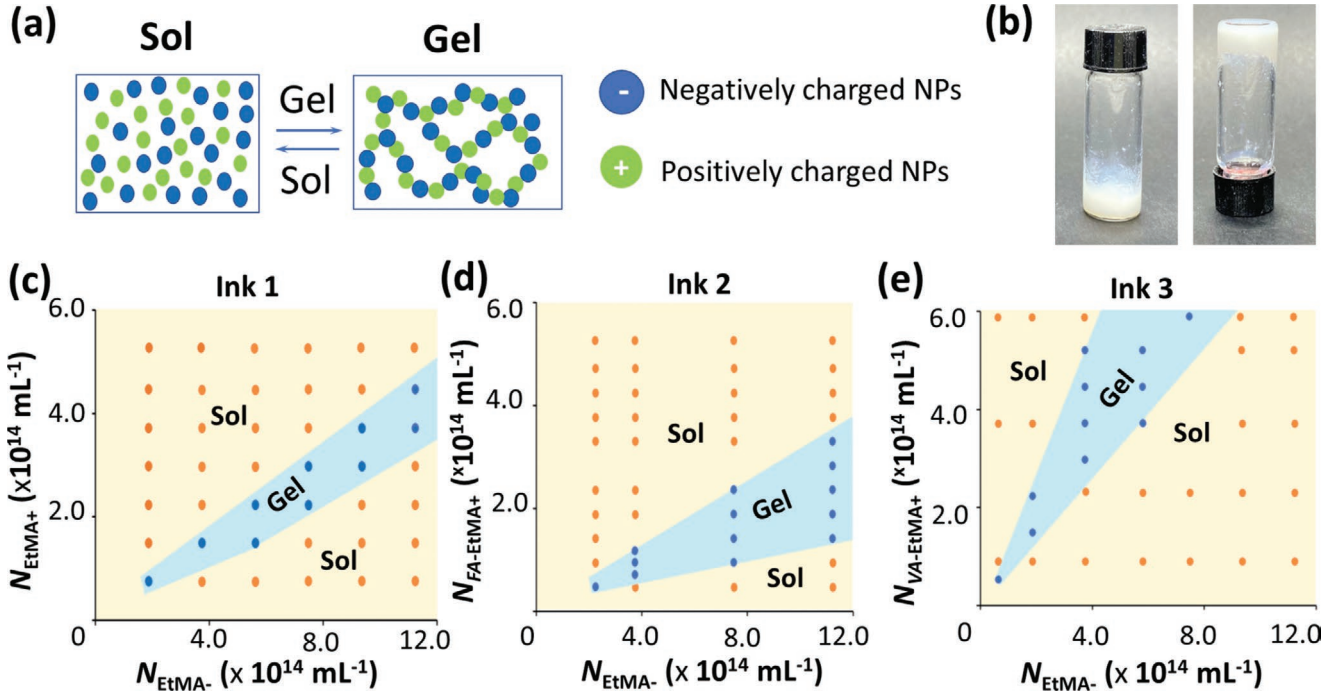

Figure 2. Preparation of nanocolloidal gel inks. a) Schematic of the formation of a nanocolloidal gel from oppositely charged NPs. b) Photograph of the gel undergoing a flip test. The gel was formed by mixing dispersions of EtMA+ and EtMA– NPs (Ink 1) at the NP number density ratio $N_{EtMA+}/N_{EtMA-} = 0.40$. c–e) State diagrams of Ink 1 (EtMA+/EtMA– NPs) (c), Ink 2 (FA-EtMA+/EtMA– NPs) (d), and Ink 3 VA-(EtMA+/EtMA– NPs) (e).

were synthesized: positively charged optically inert NPs (EtMA+ NPs), negatively charged optically inert NPs (EtMA– NPs), positively charged NPs labeled with fluorescein acrylate (FA-EtMA+ NPs), and positively charged NPs labeled with VA (VA-EtMA+ NPs). The FA-EtMA+ NPs exhibited PL emission peak at 526 nm under excitation in the spectral range of 400–480 nm, while the VA-EtMA+ NPs emitted at 428 nm when excited at 250–375 nm (Table 1).

These NPs are shown schematically in Figure 1a with green and blue colors, respectively. Table S1, Supporting Information, provides the recipes for NP synthesis. Figure 1a shows that Ink 1 was formed by mixing optically inert EtMA+ NPs and EtMA– NPs. Ink 2 was composed from a mixture of dye-labeled FA-EtMA+ NPs and optically inert EtMA– NPs. Ink 3 was a mixture of dye-labeled VA-EtMA+ NPs and optically inert EtMA– NPs (Figure S1, Supporting Information).

All NPs had electrokinetic potential, ζ-potential > |57.5| mV and narrow size distribution (except small negatively charged EtMA– NPs) (Figure S1, Supporting Information). The average hydrodynamic radius, R_h, of the NPs was 17.5 ± 8.2 nm (EtMA– NPs), 30 ± 7 nm (EtMA+ NPs), 29 ± 6 nm (VA- EtMA– NPs), and (44 ± 10) nm (FA-EtMA+ NPs) (Table 1). Charge density of latex NPs, σ, was in the range of 1.6–2.7 mC m^{-2} for positively charged NPs and –4.2 mC m^{-2} for negatively charged NPs. All NP dispersions were colloidally stable. Inks 2 and 3 were optically active. Under illumination at the excitation wavelength, λ_{ex}, of 450 nm, Ink 2 exhibited PL at emission wavelength, λ_{em}, of 526 nm (green color emission). Ink 3 exhibited blue color emission at λ_{em} = 428 nm when irradiated at λ_{ex} = 257 nm.

The results of NP imaging using scanning electron microscopy (SEM) (Figure 1b–e) were in agreement with the results of NP characterization using dynamic light scattering (DLS) (Table 1), that is, a uniform size distribution of EtMA+, FA-EtMA+, and VA-EtMA NPs and higher polydispersity of EtMA– NPs. Notably, partial NP melting and necking was observed under the electron beam, as shown in Figure 1b–e.

Figure 2a shows schematically the formation of a network (a nanocolloidal gel) from the mixture of oppositely charged NPs. At a particular ratio of concentrations of the NPs, gel formation was first, identified in a flip test (Figure 2b). A hydrogel formed immediately after NP mixing and was stable for at least, several days at room temperature. Markedly, the gelation did not depend on the order in which the dispersions of oppositely charged NPs were mixed.

Figure 2c–e shows state diagrams for three nanocolloidal inks used in the present work, with sol–gel transitions highlighted as blue regions. The number of NPs of a particular type per unit volume (1 mL) was calculated as $N = \frac{C_{NP}}{(C_{NP} + \rho/\rho_w(100 - C_{NP})) \times \frac{4}{3} \times \pi \times R_h^3}$. Here, C_{NP} is the NP mass concentration in the ink, $C_{NP} = (C_{NP}' \times V_{NP}')/V_{total}$, C_{NP}' is the NP mass concentration in the original dispersion (prior to mixing), V_{NP}' is the volume of the original dispersion, ρ_w is the density of water (1 g mL^{-1}), ρ is the density of poly(ethyl methacrylate), equal to 1.19 g cm^{-3}, and V_{total} is the total volume of the mixed dispersion.[31]

Figure 2c–e shows that for each NP mixture, the sol–gel transition occurred at a particular ratio of number densities of oppositely charged NPs, while below and above this ratio a gel was not formed. For all the three nanocolloidal gel inks, the dimensions of positively charged NPs were substantially larger than those of negatively charged NPs, with the NP size asymmetry

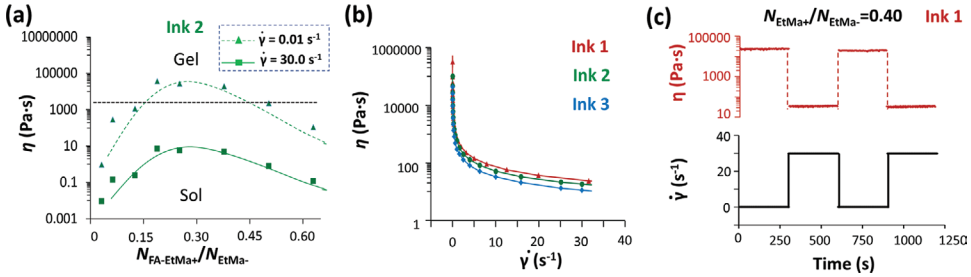

Figure 3. Rheological properties of the colloidal inks. a) Variation in shear viscosity with varying composition of Ink 2. b) Variation in shear viscosity, η, of Inks 1–3 in the gel state, plotted as a function of the shear rate $\dot{\gamma}$. c) Time-dependent variation of $\dot{\gamma}$ (bottom) and the corresponding variation in shear η of Ink 1. Ink compositions are $N_{EtMA+}/N_{EtMA-} = 0.40$ (Ink 1), $N_{FA\text{-}EtMA+}/N_{EtMA-} = 0.19$ (Ink 2), and $N_{VA\text{-}EtMA+}/N_{EtMA} = 0.88$ (Ink 3). The total NPs mass concentration in all inks was 10 wt%.

in these inks following the order Ink 2 > Ink 1 ≈ Ink 3 (Table 1). This asymmetry resulted in Ink 2 exhibiting a broader regime of network formation (Figure 2d) than Ink 1 (Figure 2c) and Ink 3 (Figure 2e). This trend was also demonstrated in mass concentration state diagrams for all three nanocolloidal inks (Figure S2, Supporting Information). We found, however, that the relative number of oppositely charged NPs that was required for network formation also depended on the asymmetry of surface charge densities of oppositely charged NPs. The asymmetry in surface charge density in three nanocolloidal gel inks followed the order Ink 2 > Ink 1 > Ink 3 (Table 1). Among three inks, Ink 2 required the largest number of negatively charged NPs for network formation, followed by Ink 1 and Ink 3 (Figure 2c–e). Since the regions corresponding to gel formation in the state diagrams outline ink compositions that are favorable for 3D printing (as we show below), the results shown in Figure 2c–e have important implications for formulating inks. More specifically, they suggest that mismatching of NP dimensions and charges may lead to a broader range of compositions of NP mixtures that can be used for 3D printing.

Hydrogel mechanical properties were further characterized in rheology experiments. **Figure 3**a shows the dependence of shear viscosity η of Ink 2 at the shear rate $\dot{\gamma}$ changing from 0.01 to 30 s^{-1}, plotted as a function of the $N_{FA\text{-}EtMA+}/N_{EtMA-}$. The value of η changed non-monotonically with varying $N_{FA\text{-}EtMA+}/N_{EtMA-}$ and reached the maximum value of ≈100 kPa s at $N_{FA\text{-}EtMA+}/N_{EtMA-} = 0.19$. This result correlated with gel formation shown in Figure 2d. The details of the relationship between NPs number density, concentration, and gelation are summarized in Table S2, Supporting Information. At $N_{FA\text{-}EtMA+}/N_{EtMA} \leq 0.13$ (a low concentration of FA-EtMA+ NPs), they were completely coated with EtMA− NPs and the clusters of oppositely charged NPs existed as individual species (corresponding to the sol state), which resulted in the low value of η. At $0.19 \leq N_{FA\text{-}EtMA+}/N_{EtMA-} \leq 0.38$, the EtMA− NPs bridged FA-EtMA+ NPs to form a network, thereby causing a transition to a nanocolloidal gel a higher viscosity (Figure S3a, Supporting Information). Further increase in $N_{FA\text{-}EtMA+}/N_{EtMA-}$ to 0.50–0.63 resulted in an insufficient number of EtMA− NPs to bridge FA-EtMA+ NPs, which led to a transition to a sol with reduced viscosity.

All gels exhibited a shear thinning behavior (Figure 3b), that is, the decrease in η with increasing shear rate, $\dot{\gamma}$, which was beneficial for 3D printing.[7] Gel viscosity greatly reduced when the shear rate $\dot{\gamma}$ increased from 0.01 to 30 s^{-1}, reaching the value of η of ≈17 +/− 7 Pa s for all gels. The variation of shear viscosity at shear rates up to 1000 s^{-1} is shown in Figure S3b, Supporting Information.

Next, we studied the recovery of η at greatly reduced $\dot{\gamma}$, that is, the "self-healing" properties of the nanocolloidal gel (Figure 3c). For Ink 1, a periodic step-wise change in $\dot{\gamma}$ between 0.05 and 30 s^{-1} resulted in the corresponding change in η of the NP mixture. Starting from $\dot{\gamma} = 0.05$ s^{-1} and $\eta = 23\,800 \pm 1300$ Pa s, an increase of $\dot{\gamma}$ to 30 s^{-1}, resulted in ≈680-fold reduction in η. Subsequent decrease of $\dot{\gamma}$ to 0.05 s^{-1} resulted in η increase to 20 200 ± 500 Pa s, that is, the recovery of 86% of the original η value. This value of η remained close to constant for 900 s. We therefore conclude that the nanocolloidal gel ink exhibited rheological properties that were highly beneficial for 3D printing: the shear thinning and rapid recovery of ink viscosity after the shear stress was reduced (leading to printing fidelity).

The mechanical properties of the films were studied by dynamic mechanical analysis (DMA) in tensile (stretching) tests of the films formed by annealing extruded nanocolloidal gels at 100 °C, that is, 34 °C above the glass transition temperature, T_g, of poly(ethyl methacrylate) of 66 °C.[34]

Figure 4a shows that the variation in elastic modulus, E_T, of all films formed from Inks 1 to 3 showed a typical frequency dependence, with a higher frequency corresponding to higher modulus[35] (Figure S4a, Supporting Information). The value of E_T for the films formed from Inks 1 to 3 increased in the order Ink 1 < Ink 2 < Ink 3. We also prepared samples by extruding Ink 1, drying it, dissolving the NPs in dimethylformamide, and casting the films. For these films, the measured E_T of 2070 MPa was approximately fourfold higher than the value of E_T of the films obtained by printing Ink 1 with the same composition (Figure S4c, Supporting Information).

The variation in the compression modulus, E_C, for all films showed a standard dependence on frequency (Figure S4b, Supporting Information). Similarly to the results shown in Figure 4a, the value of E_C increased for the films formed from Inks 1 to 3 as Ink 1 < Ink 2 < Ink 3 (Figure 4b).

To explain the difference in the mechanical properties of extruded films, their cross sections, as well as the cross sections of cast films, were imaged using SEM (Figure S5, Supporting Information). All extruded films had a porous structure, while the films cast from the solution of latex NPs (Ink 1) in dimethylformamide had a uniform structure. The area of pores

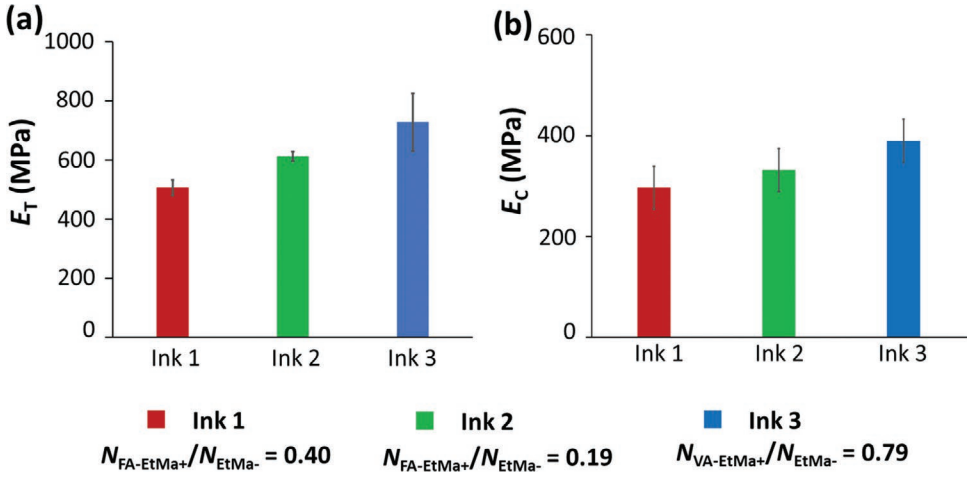

Figure 4. Mechanical properties of composite films formed from Ink 1 to 3. a) Tensile elastic modulus (E_T). b) Compression elastic modulus (E_C). The number density ratios for inks were as follows: Ink 1 ($N_{EtMA+}/N_{EtMA-} = 0.40$), Ink 2 ($N_{FA\text{-}EtMA+}/N_{EtMA-} = 0.19$), Ink 3 ($N_{VA\text{-}EtMA+}/N_{EtMA} = 0.88$).

determined by analyzing the SEM images of the films prepared by extrusion of Inks 1, 2, and 3 changed from 14% to 10% to 5%, respectively.

Therefore, we conclude that a higher value of E_T of cast films originated from their uniform structure, while in extruded films, the NPs were sintered at the temperature above polymer, T_g, and thus the network structure of the nanocolloidal inks was partly preserved in the solid films, leading to their porosity.

2.2. Optical Properties of Nanocolloidal Gel Inks

We used two criteria to select an appropriate combination of two fluorescent dyes covalently attached to the EtMA monomer to synthesize optically latex NPs, namely, i) stable dye fluorescence preserved during dye modification, covalent attachment to the monomer, and copolymerization of dye-labeled EtMA with EtMA during the synthesis of polymer particles and ii) minimal overlap in dye absorption and emission spectra of Inks 2 and 3.

Figure 5a,b shows absorption and PL emission spectra of optically active nanocolloidal gel inks, that is, Ink 2 (Figure 5a, top) and Ink 3 (Figure 5a, bottom). The corresponding excitation spectra are shown with black color, while the emission spectra are shown with red and blue colors for Inks 2 and 3, respectively. The vertical dashed lines correspond to the laser wavelengths used for excitation. Upon excitation at 375 and 480 nm, Inks 2 and 3 emitted at two distinct wavelengths, that is, at 425 and 525 nm, respectively.

Figure 5b shows images of the films formed by Inks 2 and 3, both cast on the film formed by optically inactive Ink 1. Figure 5b, top shows that at $\lambda_{ex} = 480$ nm only a green pattern

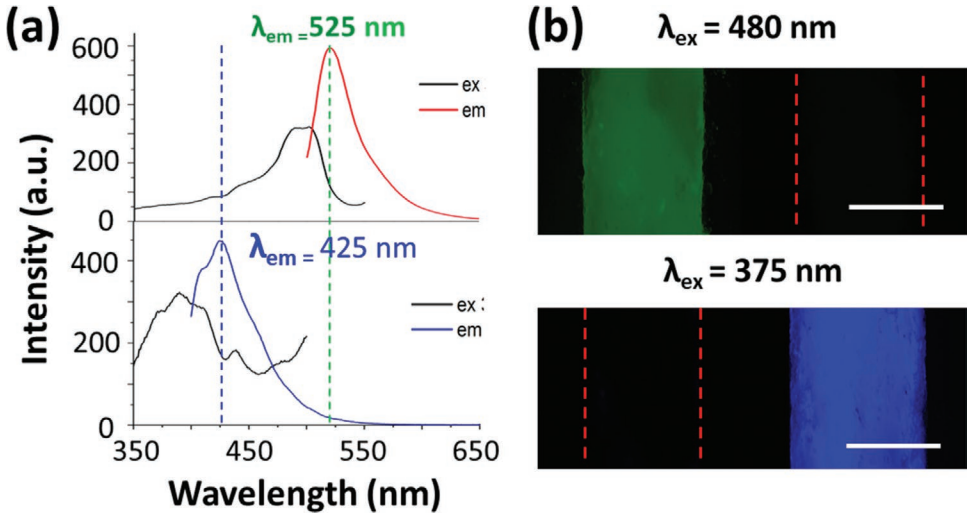

Figure 5. Optical properties of latex inks. a) Excitation and emission spectra of Ink 2 ($\lambda_{ex} = 480$ nm) (top) and Ink 3 ($\lambda_{ex} = 375$ nm) (bottom). b) Fluorescence microscopy images of the patterns formed by casting Ink 2 and 3 at $\lambda_{ex} = 480$ nm (top) and at $\lambda_{ex} = 375$ nm (bottom). The red dashed lines show the contours of the cast films that are not optically active as a specific λ_{ex}. Scale bar is 1 mm. Ink 2 and ink 3 were formed at $N_{FA\text{-}EtMA+}/N_{EtMA-} = 0.19$ and $N_{FA\text{-}EtMA+}/N_{EtMA-} = 0.88$, respectively.

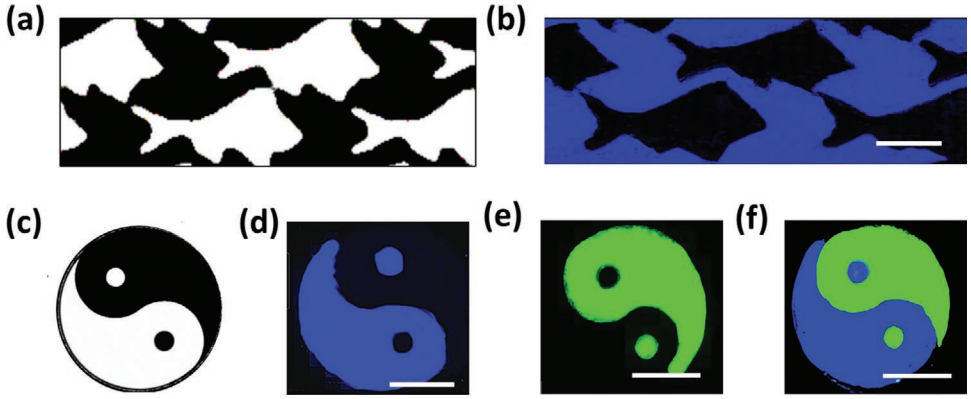

Figure 6. Printing multicolored patterns. a) Appearance of the original artwork of Maurits Escher (it was drawn using guidance provided in ref. [36]). b) Appearance of the printed Maurits pattern at λ_{ex} = 375 nm. Scale bar is 1 cm. c) Appearance of the original Yin–Yang pattern (it was drawn using guidance provided in ref. [40]). d) A PL image of the fragment of the Yin fragment of the printed Yin–Yang pattern visualized at λ_{ex} = 375 nm. e) A PL image of the Yang component of the printed Yin–Yang pattern visualized at λ_{ex} = 480 nm. f) Merged image of Ying and Yang components of the pattern. Scale bar is 1 cm.

formed by Ink 2 was visualized (Figure 5, top left), while the film formed by Ink 3 was optically inactive (Figure 5, top right). At λ_{ex} = 375 nm, a film formed by Ink 3 showed strong blue emission (Figure 5b, bottom right), while a film formed by Ink 2 was not visible (Figure 5b, bottom, left). In the latter case, partial overlap between the spectra of two inks in the 250–375 nm spectral range was compensated by reducing irradiation intensity at λ_{ex} = 375 nm (Figure S6, Supporting Information).

2.3. Printing Multicolored Patterns

To show the capability to print complex patterns, we combined nanocolloidal gel Inks 1 and 3 to print a 1.5 cm × 8.5 cm film with the tessellation pattern of birds and fish (the artwork of Maurits Escher)[36] **Figure 6**a). The fish pattern was printed using an optically inert Ink 1, while the bird pattern was printed using Ink 3. Figure 6b shows that under λ_{ex} = 375 nm, the fish pattern appeared black, while the swan pattern appeared blue, due to the VA dye emission at 428 nm. A similar result was obtained by combining Inks 1 and 2 (Figure S7, Supporting Information).

Since NP diameters were in the range from 35 to 88 nm and the dimensions of the smallest extruded feature was equal or above 500 µm, the fluorescence colors in the multicolor pattern were not affected by NPs dimensions. Notably, the maximum intensities of fluorescence emission of VA- and VA-labeled NPs were comparable.

Next, we used Inks 1–3 to print multicolored patterns. We reproduced the Yin–Yang pattern with diameter 2.2 cm (Figure 6c). An optically inactive black background was printed with Ink 1. The Yin fragment was then printed using Ink 2 and visualized at λ_{ex} = 480 nm (Figure 6e), while Ink 3 was optically inactive at this λ_{ex}. The Yang component of the pattern was printed using Ink 3 and visualized at λ_{ex} = 375 nm (Figure 6d), while Ink 2 was not visible at this λ_{ex}. We note that after extrusion and during liquid layer drying, partial mixing of latex NPs of Inks 2 and 4 occurred at the interface between the Yin and Yang components of the pattern, which resulted in ≈100 µm-thick light-blue interfacial layer in the overlay image of the dry film with Yin–Yang pattern (Figure 6f).

Our work outlines important criteria for development of functional nanocolloidal hydrogel inks for extrusion-based 3D printing. The results shown in Figures 2 and 3 show that weak physical gels with shear thinning properties form only in a particular range of ink compositions. More specifically, the formation of colloidal networks by electrostatic interactions of oppositely charged NPs occurs in a specific range of NP charges and dimensions, which affects the "symmetry" of state diagrams with respect to the NP number densities. A broader range of nanocolloidal gel ink formulations is achieved when the dimensions of counterpart NPs are mismatched. This observation is consistent with previously reported results from molecular dynamic simulations of percolation of size- and charge-asymmetric oppositely charged colloidal particles.[37] According to this study, the size and charge asymmetry in mixtures of oppositely charged particles affects the structure of clusters and their distribution in the network, which eventually, determines the properties of the colloidal hydrogel. Therefore, fine-tuning the surface charge and particle size is imperative for designing inks with desired properties from colloidal particles.

For polymer NPs, film formation from hydrogel inks occurs at the temperature above the glass transition temperature, T_g, of the polymers.[38] In the present work, the T_g of the polymer was 66 °C,[34] which necessitated post-extrusion heating of the layer of latex NPs. Nevertheless, the mechanical properties of the printed films were inferior to those formed from the corresponding polymer solutions. Post-extrusion film heating may cause polymer diffusion between different regions of the film, which would reduce the resolution and quality of printing of structurally and compositionally heterogeneous materials with, for example, multicolored features. Furthermore, to print materials with specific optical properties, the chromophores should retain their properties at elevated temperatures. Based on these considerations, it is desirable to use polymer with moderately high values of T_g and if needed, use photocross-linking to enhance the mechanical properties of the material.

With regards to the use of optically active species, for example, dyes, it is highly desirable to avoid spectral overlap in their excitation and emission spectra to print compositionally heterogeneous materials. Covalent attachment of dyes to the monomers is desirable to avoid dye diffusion and phase separation, thereby enabling dye localization in respective NPs and thus specific regions of printed films. Finally, we admit the possibility of non-radiative energy transfer at the interface of the regions containing different dyes, however it is limited to a narrow region of ≈10 nm,[39] which is well below the 580 µm (20G nozzle), the dimensions of features extruded in the present work.

3. Conclusion

Our work has several important implications. First, by using oppositely charged latex NPs, we show the approach to the generation of functional (multicolored) nanocolloidal gel inks. Second, we show that the formation of the physical shear-thinning gel (used as inks for 3D printing) occurs in a specific range of ratios of number densities of the counterpart NPs, which depends on NP charge density and dimensions. Third, we propose an approach to 3D printing of millimeter-resolution multicolored fluorescence patterns, with each of color visualized at a particular excitation wavelength. Finally, we discuss the criteria and considerations for the development of polymer-based functional (multicolored) nanocolloidal inks.

4. Experimental Section

Chemicals and Materials: EtMA (99%), SDS (99%), hexadecyltrimethylammonium bromide (CTAB, 99%), KPS (99%), VA (97%), and ethylene glycol (99%) were purchased from Aldrich and used as received. V-50 (98%) was supplied by Acros Ltd. Fluorescein acrylate was synthesized according to the previously reported procedure.[31]

Synthesis of Latex Nanoparticle: *Synthesis of positively charged latex particles*: Latex NPs were synthesized in a semi-continuous "seed-and-feed" process. EtMA (3.5 mL) was emulsified in 55 mL of deionized water containing 50 mg of CTAB. The suspension was heated to 80 °C and purged with Ar for 30 min. Under stirring provided by a mechanical stirrer at 300 rpm, a solution of 60 mg of V-50 in 5 mL of water was injected to the suspension at a rate of 0.5 mL min^{-1}. After 1 h, 10 mL of EtMA and a solution of 40 mg of V-50 and 150 mg of CTAB in 25 mL of water, were injected to the polymerization flask at a rate of 1.0 and 2.5 mL min^{-1}, respectively. After 20 h, the polymerization was stopped, and the latex NP dispersion was purified by dialysis against deionized water for 5 days using 3.5 kDa membrane.

Synthesis of negatively charged latex NPs: Latex NPs were synthesized in a continuous process, in which the 7.5 mL of EtMA was emulsified in 55 mL of deionized water containing 1 g of SDS. The emulsion was heated to 80 °C and purged with Ar gas for 30 min. Under stirring provided by a mechanical stirrer at 300 rpm, a solution of 60 mg of KPS in 5 mL of water was injected to the suspension at a rate of 0.5 mL min^{-1}. The solution was then stirred at 80 °C for 2 h. The latex dispersion was purified by dialysis against deionized water for 5 days using 3.5 kDa membrane.

Synthesis of positively charged FA-labeled latex NPs: Latex NPs were synthesized in a semi-continuous "seed-and-feed" process. First, 3.5 mL of EtMA was emulsified in 55 mL of deionized water containing 50 mg of CTAB. The emulsion was heated to 80 °C and purged with Ar gas for 30 min. Under stirring provided by a mechanical stirrer at 300 rpm, a solution of 60 mg of V-50 in 5 mL of water was injected to the suspension at a rate of 0.5 mL min^{-1}. After 1 h of polymerization, a solution of 50 mg of FA in 10 mL of EtMA and a solution of 40 mg of V-50 and 150 mg of CTAB in 25 mL of water were injected to the polymerization flask at a rate of 1 and 2.5 mL min^{-1}, respectively. After 20 h, the polymerization was stopped, and the latex NP dispersion was purified by dialysis against deionized water for 5 days in 3.5 kDa membrane.

Synthesis of negatively charged VA-labeled latex NPs: Latex NPs were synthesized in a continuous process, in which 50 mg of VA was dissolved in 7.5 mL of EtMA. The monomer mixture was emulsified in 55 mL of deionized water containing 1 g of SDS. The suspension was heated to 80 °C and purged with Ar for 30 min. Under stirring provided by a mechanical stirrer at 200 rpm, a solution of 60 mg of KPS in 5 mL of water was injected to the suspension at a rate of 0.5 mL min^{-1}. The solution was then stirred at 80 °C for 2 h. The latex NP dispersion was purified by dialysis against deionized water for 5 days using 3.5 kDa membrane.

Characterization of Latex Nanoparticles: The electrokinetic potentials (ζ-potential) and the hydrodynamic diameter of latex NPs were determined using DLS (Malvern Zetasizer Nano ZS instrument ZEN3600 instrument). Experiments were performed at 22 °C in triplicate format, and the correlation data was analyzed by the built-in Malvern General Purpose non-negative least squares method. Imaging of NPs was performed using SEM (Carl Zeiss CrossBeam 1540XB/Cross-beam SEM-FIB workstation Carl Zeiss CrossBeam 1540XB) at 5.00 kV. The samples were prepared by depositing a drop of 10 µg mL^{-1} latex NP dispersion on silicone substrate and drying it at 45 °C for 30 min. EtMA–NPs were additionally coated with carbon for better contrast.

Construction of state diagrams for mixtures of latex dispersions: To study sol–gel transitions for latex NP mixtures, a dispersion of negatively charged NPs was added with a step of 10 µL to 100 µL of positively charged NPs. The concentration of NPs in each original dispersion was 10 wt%. After each step, the mixture was stirred for 1 min and flip tests were performed to evaluate the state of the mixture.

Rheology experiments: A rheometer (Discovery Hybrid Rheometer, DHR-2, TA Instruments, USA) with a cone of 0.97° (diameter: 40 mm) and a gap of 27 µm were used to study the rheological properties of the inks. To control the temperature and to minimize solvent evaporation, an integrated Peltier plate and a solvent trap were used, respectively. To measure the viscosity at different shear rates, the inks were equilibrated for 600 s at 22 °C, followed by a flow ramp experiment, in which the shear rate varied from 0.01 to 30.0 s^{-1}. Self-healing properties of inks were studied using shear rate oscillation experiments. A single cycle consisted of the measurement of shear viscosity at $\dot{\gamma}$ = 0.05 s^{-1} for 10 min, equilibration for 10 min, and the measurement of shear viscosity at $\dot{\gamma}$ = 30.0 s^{-1} with a step duration of 5 min.

Characterization of PL properties of latex NP dispersions: Studies of fluorescence of latex NP dispersions were conducted using a spectrophotometer (Cary 8454 UV-Vis, Santa Clara, CA, USA). Emission spectra of VA-labeled NPs are in agreement with previously reported data.[33]

Dynamic mechanical analysis: DMA was performed on NETZSCH DMA 242 E Artemis (Germany) at 25 °C in the tension and compression mode. To the elastic tensile modulus, E_T, film with dimensions of 5 mm × 15 mm and thickness in range of 40–80 µm were cut from the printed films. To measure the elastic compression modulus, E_C, of the films, the inks were extruded in a silicone mold, dried at r.t. for 8 h for removing water and processed by hot pressing at 120 °C to obtain 2 mm-thick films. The diameter of the indenter in the compression mode was 3 mm. Table S4, Supporting Information, lists the details of the characterization of the mechanical properties of the films. The elastic modulus E_T (tensile test) and E_C (compression test) were obtained at frequencies of 1, 10, and 100 Hz and a constant temperature T = 25 °C.

Fluorescent microscopy: All optically active patterns were visualized using a fluorescence microscope Leica DMi8 equipped with a Leica DFC365FX digital camera (Leica, Germany) under bright field, fluorescent filter cubes: DAPI (excitation wavelength = 325–375 nm, emission wavelength = 435–485 nm), FITC (excitation wavelength 460–500 nm, emission wavelength 512–542 nm). The printed patterns were scanned in mosaic capture mode.

3D Printing: All inks were printed using pneumatic Cellink Bio X printer with conic needles 20G (0.58 mm) on glass substrate. For

improving printability of inks, ethylene glycole was added to the each ink at 2 wt% concentration. The optically active patterns were designed using Tinkercad software, and converted to G-code that was optimized in Cellink Heartware software (version 2.4.1). The optimized inks printing parameters are shown in Table S5, Supporting Information, respectively. The printing speed was 40 mm s^{-1}, while the pressure varied from 8 to 15 kPa, depending on the type of the ink (Table S5, Supporting Information). The temperature of the ink was 20–22 °C, while the temperature of the substrate was 16 °C.

Supporting Information

Supporting Information is available from the Wiley Online Library or from the author.

Acknowledgements

The research was carried out in collaboration. S.M.M., T.G.S., and A.V.K. acknowledge the Russian Science Foundation (Project No 21-79-20113) for supporting the studies on latex synthesis, mechanical characterization, and SEM imaging. E.O.R. and E.K. acknowledge the Ministry of Science and Higher Education of the Russian Federation (Project No. 075-15-2019-1896) for supporting the studies on fluorescent microscopy and printing. NSERC Canada (Discovery grant program) is acknowledged for the support of research carried out in Canada. E.K. thanks NSERC Canada Research Chair (Tier 1) program. A.G. acknowledges support from NSERC CREATE Training Program in Organ-on-a-chip Engineering and Entrepreneurship (TOeP). This work was in part carried out using equipment of the SPbU Resource Centers "Nanophotonics" and "Nanotechnology".

Conflict of Interest

The authors declare no conflict of interest.

Data Availability Statement

Research data are not shared.

Keywords

colloidal inks, fluorescent coatings, fluorescent dyes, latex nanoparticles, shear-thinning, three-dimensional printing

Received: June 7, 2021
Revised: July 29, 2021
Published online: September 29, 2021

[1] H. Ragelle, M. W. Tibbitt, S.-Y. Wu, M. A. Castillo, G. Z. Cheng, S. P. Gangadharan, D. G. Anderson, M. J. Cima, R. Langer, *Nat. Commun.* **2018**, *9*, 1184.
[2] E. Prince, E. Kumacheva, *Nat. Rev. Mater.* **2019**, *4*, 99.
[3] S. A. Wilson, L. M. Cross, C. W. Peak, A. K. Gaharwar, *ACS Appl. Mater. Interfaces* **2017**, *9*, 43449.
[4] Y. Wu, Z. Yuan, W. Lin, C. Andrew, K. C. Tam, X. S. Tang, *Bioprinting* **2017**, *9*, https://doi.org/10.1016/j.bprint.2017.12.001.
[5] E. A. Appel, M. W. Tibbitt, M. J. Webber, B. A. Mattix, O. Veiseh, R. Langer, *Nat. Commun.* **2015**, *6*, 6295.
[6] A. Gevorkian, S. M. Morozova, S. Kheiri, N. Khuu, H. Chen, E. Young, N. Yang, E. Kumacheva, *Adv. Funct. Mater.* **2021**, *31*, 2010743.
[7] N. Khuu, M. Alizadehgiashi, A. Gevorkian, E. Galati, N. Yan, E. Kumacheva, *Adv. Mater. Technol.* **2019**, *4*, 1800627.
[8] A. Khabibullin, M. Alizadehgiashi, N. Khuu, E. Prince, M. Tebbe, E. Kumacheva, *Langmuir* **2017**, *33*, 12344.
[9] I. Donderwinkel, J. C. M. Van Hest, N. R. Cameron, *Polym. Chem.* **2017**, *8*, 4451.
[10] C. B. Highley, K. H. Song, A. C. Daly, J. A. Burdick, *Adv. Sci.* **2019**, *6*, 1801076.
[11] C. Zhu, A. J. Pascall, N. Dudukovic, M. A. Worsley, J. D. Kuntz, E. B. Duoss, C. M. Spadaccini, *Annu. Rev. Chem. Biomol. Eng.* **2019**, *10*, 17.
[12] M. Zeng, Y. Zhang, *J. Mater. Chem. A* **2019**, *7*, 23301.
[13] E. MacDonald, R. Wicker, *Science* **2016**, *353*, aaf2093.
[14] S. Patra, V. Young, *Cell Biochem. Biophys.* **2016**, *74*, 93.
[15] R. Kikuchi, S. Yoshikawa, P. K. Jayaraman, J. Zheng, T. Maekawa, *Comput. Aided Des.* **2018**, *102*, 215.
[16] L. Y. Zhou, J. Fu, Y. He, *Adv. Funct. Mater.* **2020**, *30*, 2000187.
[17] Z. Nie, E. Kumacheva, *Nat. Mater.* **2008**, *7*, 277.
[18] M. K. Hausmann, P. A. Ruhs, G. Siqueira, J. Läuger, R. Libanori, T. Zimmermann, A. R. Studart, *ACS Nano* **2018**, *12*, 6926.
[19] W. Xue, G. S. Grest, *Phys. Rev. Lett.* **1990**, *64*, 419.
[20] Z. Chen, X. Hu, X. Wang, Z. Xiang, *RSC Adv.* **2020**, *10*, 4949.
[21] Y. Han, L. Su, L. Mao, L. Zhang, D. Yue, *Polym.-Plast. Technol. Eng.* **2014**, *53*, 306.
[22] Y. Zang, J. Du, Y. Du, Z. Wu, S. Cheng, Y. Liu, *Langmuir* **2010**, *26*, 18331.
[23] I. Konko, S. Guriyanova, V. Boyko, L. Sun, D. Liu, B. Reck, Y. Men, *Langmuir* **2019**, *35*, 6075.
[24] M. Soleimani, J. C. Haley, D. Majonis, G. Guerin, W. Lau, M. A. Winnik, *J. Am. Chem. Soc.* **2011**, *133*, 11299.
[25] H. H. Pham, I. Gourevich, E. N. Jonkman, E. Kumacheva, *J. Mater. Chem.* **2007**, *17*, 523.
[26] B. J. Siwick, O. Kalinina, E. Kumacheva, R. J. D. Miller, J. Noolandi, *J. Appl. Phys.* **2001**, *90*, 5328.
[27] Y. Zhang, X. Le, Y. Jian, W. Lu, J. Zhang, T. Chen, *Adv. Funct. Mater.* **2019**, *29*, 1905514.
[28] H. H. Pham, I. Gourevich, J. K. Oh, J. E. N. Jonkman, E. Kumacheva, *Adv. Mater.* **2004**, *16*, 516.
[29] X. Cui, C. Zhang, R. P. Camilo, H. Zhang, A. Cobaj, M. D. Soucek, N. S. Zacharia, *Macromol. Mater. Eng.* **2018**, *303*, 1700596.
[30] S. De Siqueira, R. Fleury, M. Fabrício, F. Rosa, M. Augusto, M. Fonseca, G. Virgolino, C. Federico, D. Avila, A. Guimarães, D. Domínguez, A. Guimarães, D. Dantas, V. B. Richter, *J. Diabetes Res.* **2019**, *2019*, https://doi.org/10.1155/2019/7457295.
[31] P. J. Scott, V. Meenakshisundaram, M. Hegde, C. R. Kasprzak, C. R. Winkler, K. D. Feller, C. B. Williams, T. E. Long, *ACS Appl. Mater. Interfaces* **2020**, *12*, 10918.
[32] M. Lukic, J. Clarke, C. Tuck, W. Whittow, G. Wells, *J. Appl. Polym. Sci.* **2016**, *133*, https://doi.org/10.1002/app.42931.
[33] H. Thérien-aubin, A. Lukach, N. Pitch, E. Kumacheva, *Nanoscale* **2015**, *7*, 6612.
[34] J. A. Roetling, *Polymer* **1965**, *6*, 615.
[35] D. J. Hourston, F. U. Schäfer, *Polymer* **1996**, *37*, 3521.
[36] M. C. Escher, *MC Escher: The Graphic Work*, Taschen, Cologne, Germany **2000**.
[37] K. Singh, A. Raghav, P. K. Jha, S. Satapathi, *Sci. Rep.* **2019**, *9*, https://doi.org/10.1038/s41598-019-40379-y.
[38] J. W. Vanderhoff, *Polym. News* **1977**, *3*, 194.
[39] F. M. Raymo, M. Tomasulo, *Chem. Soc. Rev.* **2005**, *34*, 327.
[40] C. Browne, *Computers & Graphics* **2007**, *31*, 142.